



# A nano sensor for sensitive and selective detection of $\text{Cu}^{2+}$ based on fluorescein: Cell imaging and drinking water analysis

Prasad G. Mahajan<sup>a</sup>, Nilam C. Dige<sup>b</sup>, Balasaheb D. Vanjare<sup>a</sup>, Seong-Hui Eo<sup>b</sup>, Song Ja Kim<sup>b</sup>, Ki Hwan Lee<sup>a,\*</sup>

<sup>a</sup> Department of Chemistry, Kongju National University, Gongju, Chungnam 32588, Republic of Korea

<sup>b</sup> Department of Biological Sciences, Kongju National University, Gongju, Chungnam 32588, Republic of Korea

## ARTICLE INFO

### Article history:

Received 9 January 2019

Received in revised form 9 March 2019

Accepted 9 March 2019

Available online 11 March 2019

### Keywords:

Fluorescein

Organic nanoparticles

Chelation enhanced fluorescence (CHEF)

$\text{Cu}^{2+}$  sensing

Drinking water

Cell imaging

## ABSTRACT

A fluorescein-based nano probe was designed and synthesized for ultra-sensitive detection of  $\text{Cu}^{2+}$  in aqueous solution. The formation of fluorescent organic nanoparticles confirmed by using particle size analysis and scanning electron microscopy. UV–Vis. absorption and fluorescence spectroscopy displays excellent photophysical properties of prepared nanoparticles as compared to parent molecule *i.e.* N-(3',6'-dihydroxy-3-oxo-3,3a-dihydrospiro[isindole-1,9'-xanthene]-2(7aH)-yl)-1-naphthamide (FNH) in acetone. A series of 18 metal ion was examined with FNH nanoparticles (FNHNPs) to examine the change in fluorescence response. Pleasingly, only copper ion ( $\text{Cu}^{2+}$ ) shows selective and sensitive fluorescence enhancement effect, which discussed on chelation-enhanced fluorescence phenomenon. Other competing metal ions does not affect the FNHNPs fluorescence enhancement induced by  $\text{Cu}^{2+}$  ion. The excited state complexation through chelation-enhanced fluorescence of FNHNPs was further supported by UV–Vis. absorption and fluorescence decay titration of FNHNPs with and without the addition of  $\text{Cu}^{2+}$ . The present investigation approach serves extremely low detection limit of 1.62 ng/mL (0.024  $\mu\text{M}$ ) for  $\text{Cu}^{2+}$  in aqueous solution. In addition, benefit of present study includes practical application for the quantitative estimation of  $\text{Cu}^{2+}$  in drinking water sample and intracellular cell imaging for  $\text{Cu}^{2+}$ .

© 2019 Elsevier B.V. All rights reserved.

## 1. Introduction

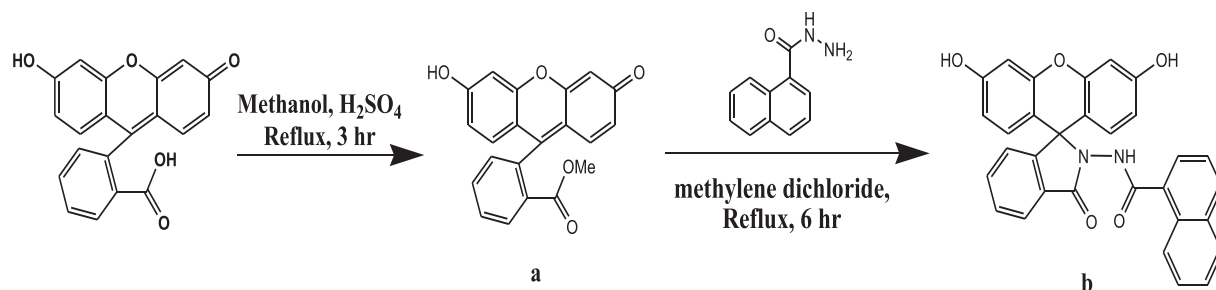
The chemosensor for ultrasensitive detection of heavy metal ion based on fluorescence output has acknowledged much more attention in last few decades [1–4]. The number of heavy metal ions is essential in human body for natural growth and stimulation of metabolism process [5–8]. Amongst the series of heavy metal ion, copper ion ( $\text{Cu}^{2+}$ ) is one of the crucial metal ions, which acts as micronutrient for human being and plants. It plays a vital role in different metalloenzymes, human nervous system, gene expression, protein functioning and biological systems of plants [9,10]. Nevertheless, a higher dose of  $\text{Cu}^{2+}$  ions may produce ill effect in the form of neurodegenerative disorders such as amyotrophic lateral sclerosis, Parkinson's, Alzheimer's, Wilson's and Menke's diseases [9,11–13]. There may be a possibility of damage of kidney damage gastrointestinal disorders due to excess intake of  $\text{Cu}^{2+}$  than permissible level in human body [14]. The shortage of  $\text{Cu}^{2+}$  induces effect on human health and lead to anemia and arteriosclerosis [10]. In addition, lack of effective wastewater management increases the pollution caused by  $\text{Cu}^{2+}$  in water in most of the countries over the world. The U.S. Environmental Protection Agency (EPA) established

20  $\mu\text{M}$  as safe and higher concentration limit for  $\text{Cu}^{2+}$  in drinking water [14,15]. Therefore, the detection of  $\text{Cu}^{2+}$  is highly essential as far as health and environment issues are concerns.

The efforts have been dedicated to design and construct a selective and sensitive chemosensor for  $\text{Cu}^{2+}$  in an aqueous solution using number of compounds from different class of fluorescent family such as rhodamine [5,7–9,13,16,17], coumarin [15], fluorescein [18–20], dansyl [21,22] and anthracene [23,24]. The different analytical methods based on electrochemical techniques [25,26], colorimetric detection [10,16,17,27], atomic absorption spectroscopy [28,29], chemiluminescence process [30,31], inductively coupled plasma atomic emission spectroscopy [32,33], fluorescence spectroscopy [1,9,11–17] and inductively coupled plasma-mass spectroscopy [34,35] are widely used for the detection of  $\text{Cu}^{2+}$  in aqueous solutions. Amongst them, fluorescence-based sensing techniques are highly desirable due to the simplicity in operation process, quick response, sensitive and selective binding towards desired analyte molecule, minimize the effect of competing ions, does not requires preparation of additional reagents and most important offers ultra-trace detection limit. However, other mentioned techniques are fails to produce such desirable outputs and eventually hurdles in the quantitative determination of metal ion in aqueous solution. The hydrophilic characters of compound play a significant role in designing the chemosensor for detection of heavy metal ion in

\* Corresponding author.

E-mail address: [khlee@kongju.ac.kr](mailto:khlee@kongju.ac.kr) (K.H. Lee).



**Scheme 1.** Synthesis of FNH.

aqueous medium. The number of reports witnessed for the detection of metal ion using mixed organo-water or buffered system because of hydrophobic characteristics posed by fluorescent organic compounds [9,10,16,27]. Nowadays, the highly grown emerging research field has been adopted namely fluorescent organic nanoparticles for the elimination of drawbacks postured by traditional analytical methods. Specially, the sensing method based on fluorescent organic nanoparticles (FONs) prepared by using small weight compounds is advantageous because of highly selective and sensitive response, ease of preparation and lower detection limit over traditional methods and direct use of fluorescent molecules in aqueous medium [36–41]. Therefore, the design and synthesis of FONs and their utility for sustainable environment is still challenging research area in scientific community.

Herein, we synthesized a small fluorescein based compound namely *N*-(3',6'-dihydroxy-3-oxo-3,3a-dihydrospiro[isoindeole-1,9'-xanthen]-2(7aH)-yl)-1-naphthamide (FNH) to explore as nano sensor for detection of heavy metal ion in aqueous solution. Pleasingly, the prepared nanoparticles (FNHNPs) shows highly selective and sensitive fluorescence enhancement with addition of  $\text{Cu}^{2+}$  ion only, due to chelation enhanced fluorescence phenomenon (CHEF). The present analytical approach was successfully applied for the quantitative determination of  $\text{Cu}^{2+}$  ion in drinking water and intracellular cell imaging of  $\text{Cu}^{2+}$  for two-cell lines viz. MDA-MB-231 and A375.

## 2. Experimental

### 2.1. Materials

Fluorescein and 1-naphthoic hydrazide were procured from Sigma Aldrich. All other reagents and solvents such as acetone, methanol, methylene dichloride and ethanol of analytical grade were purchased from Samchun Chemicals, Korea. All salts for metal ion solution were

purchased from Alfa Aesar. Double distilled water was used to carry out all sensing experiments. The MDA-MB-231 and A375 cell lines were obtained from American Type Culture Collection (ATCC, Rockville, MD, USA). Fetal bovine serum (FBS) and Dulbecco modified eagle medium (DMEM) were purchased from Gibco (Carlsbad, CA, USA). MTT (5-dimethylthiazol-2-yl-2,5-diphenyltetrazolium bromide) was procured from Sigma Aldrich. All other chemicals and reagents were obtained from Sigma Aldrich until and unless mentioned.

### 2.2. Methods

#### 2.2.1. Synthesis of compound FNH

**2.2.1.1. Synthesis of methyl 2-(8a, 9-dihydro-3-hydroxy-6-oxo-6H-xanthen-9-yl) benzoate (compound a).** The already reported method [42] was followed for the synthesis of **compound FNH**. The Fluorescein (1.03 g, 3.1 mmol) in methanol solution (50 mL) was equipped in 100 mL round bottom flask followed by addition of 2.2 mL of conc.  $\text{H}_2\text{SO}_4$ . The whole mixture was stirred and refluxed for 3 h. The reaction process was monitored using TLC. After endorsing the completion of reaction, it allowed to cool at ambient temperature and then evaporated under reduced pressure. The obtained brown-red solid was further washed with distilled water to avoid the existence of unreacted starting material. The crude solid of fluorescein methyl ester (**compound a**) was filtered, dried and offered in 91% yield which further used to synthesize **compound b-FNH** i.e. *N*-(3',6'-dihydroxy-3-oxo-3,3a-dihydrospiro[isoindeole-1,9'-xanthen]-2(7aH)-yl)-1-naphthamide.

**2.2.1.2. Synthesize of *N*-(3',6'-dihydroxy-3-oxo-3,3a-dihydrospiro[isoindeole-1,9'-xanth-ene]-2-(7aH)-yl)-1-naphthamide (compound b-FNH).** A mixture of compound **a** (0.69 g, 2 mmol) and 1-naphthoic hydrazide (0.39 g, 2.1 mmol) in 20 mL methylene dichloride was stirred

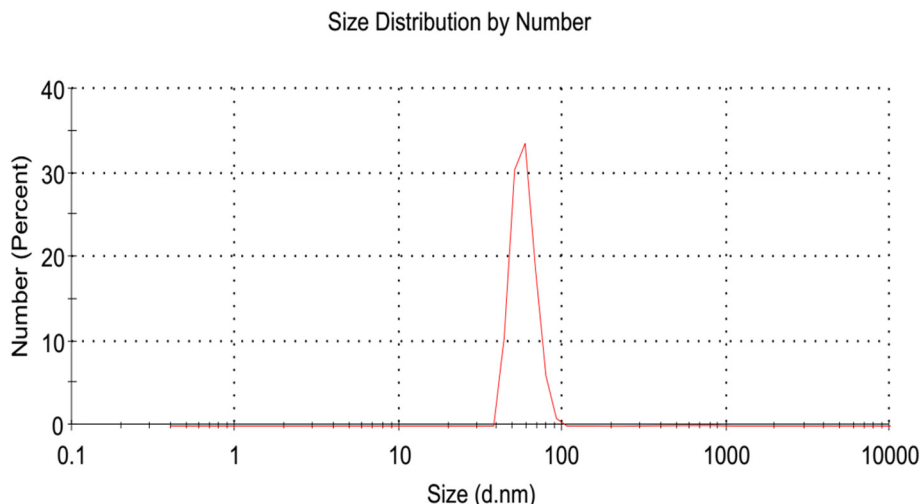


**Fig. 1.** Particle size distribution curve of FNHNPs.

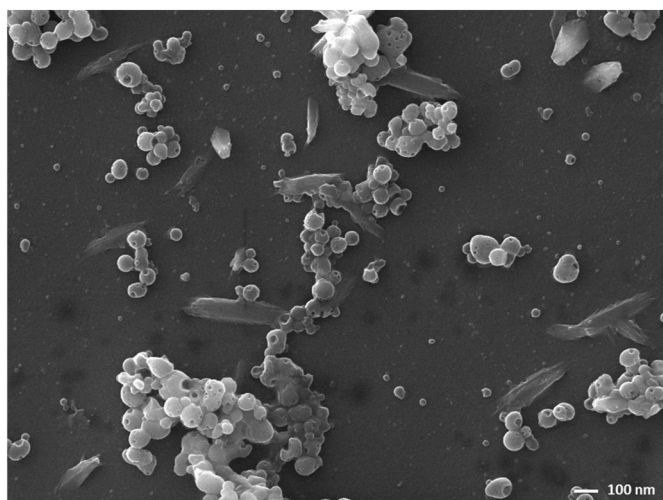


Fig. 2. FE-scanning electron microphotograph of FNHNPs.

and refluxed for 6 h. The completion of reaction was confirmed using TLC. After 6 h, reaction mixture was allowed to cool at room temperature and solvent was evaporated under reduced vacuum pressure. Thus, orange-yellow powder obtained in appreciable 84% yield (0.809 g) was recrystallized by using hot ethanol. The recrystallized product of **compound b-FNH** was further analyzed using characterization techniques viz., IR, NMR and mass spectroscopy. The schematic route of FNH shown in Scheme 1. M.P.: Observed: 141–144 °C; IR Fig. S1: 2922 (—NH & OH), 1714, 1637 (C=O), 1588, 1539, 1455, 1380, 1265, 1162, 1114, 1081, 1054, 996, 919, 848, 753, 704, 664  $\text{cm}^{-1}$ ;  $^1\text{H}$  NMR (DMSO- $d_6$ , 400 MHz) Fig. S2  $\delta$ : 10.37 (s, 2H, —OH), 8.27 (s, 4H, ArH), 7.83–7.92 (m, 5H, ArH), 7.53 (s, 2H, ArH), 7.11 (s, 3H, ArH), 6.89 (s, 2H, ArH), 6.67 (s, 1H, ArH), 6.56 (s, 1H, —NH) ppm;  $^{13}\text{C}$  NMR (DMSO- $d_6$ , 100 MHz) Fig. S3  $\delta$ : 165.65 (C=O), 137.80, 131.71, 125.12, 55.92 (spiro carbon); mass (ESI MS) Fig. S4: 501.4 [M+1]  $m/z$ .

### 2.2.2. Synthesis of FNH nanoparticles (FNHNPs)

The simple and cost effective reprecipitation method was used to prepare an aqueous suspension of fluorescent organic nanoparticles of FNH [41–43]. In this process, a 2 mL,  $5 \times 10^{-4}$  M FNH solution prepared in acetone was rapidly injected into flask containing 100 mL double distilled water. The solution was stirred vigorously for 45 min on magnetic stirrer. Further, the solution was sonicated for 15 min at 40 °C. Thus,

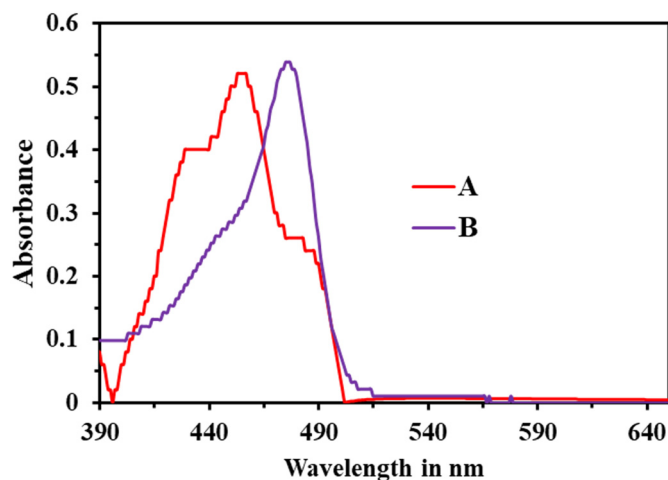


Fig. 3. Absorption spectra of dilute solution of FNH in acetone (A) and aqueous suspension of FNHNPs (B).

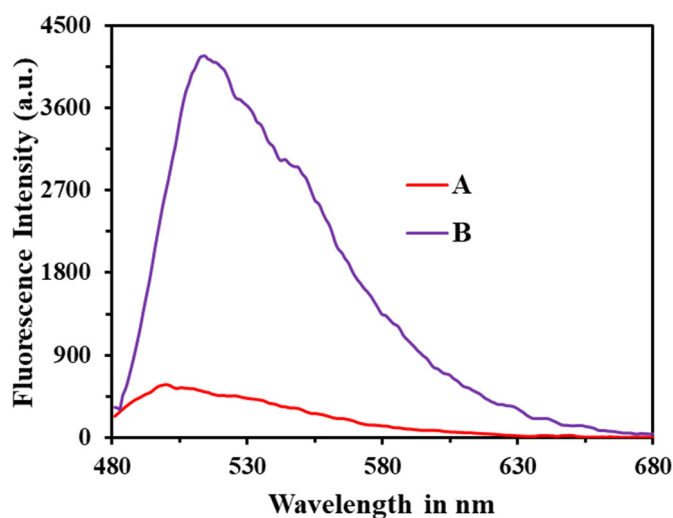


Fig. 4. Fluorescence emission spectra of dilute solution of FNH in acetone (A) and aqueous suspension of FNHNPs (B).

dark fluorescent straw yellow colored aqueous suspension of nanoparticles ( $1 \times 10^{-5}$  M) was obtained and which was further used to check their photophysical properties and sensing experiment.

### 2.2.3. Characterization techniques

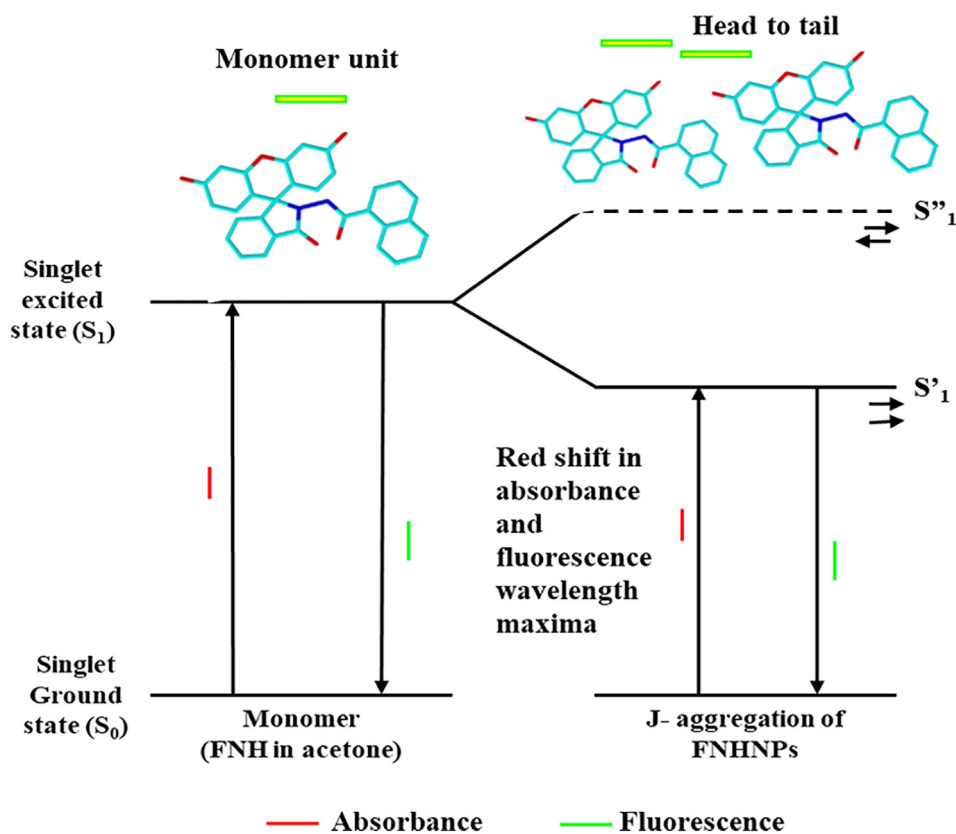
The melting point of compound was determined on Fisher Scientific (USA) melting point apparatus. The Frontier IR (Perkin Elmer) spectrometer was used to examine the FT-IR spectrum in KBr pellets. The Bruker Avance 400 MHz spectrometer with TMS as an internal standard was used for scanning  $^1\text{H}$  NMR (400 MHz) and  $^{13}\text{C}$  NMR (100 MHz) spectra. The LC-MS was examined on 2795/ZQ2000 (waters) spectrometer. The zeta potential and particle size of nanoparticles was inspected under Malvern Zeta-Particle size analyzer based on Dynamic light scattering technique. The morphology of nanoparticles assessed using FE-SEM (MIRA3 LMH, TESCAN, USA). The Shimadzu Spectrophotometer (Japan) and FS-2 fluorescence spectrophotometer (Scinco, Korea) was used for examining the UV–visible absorption and Fluorescence spectra, respectively in respective solvents. The lifetime decay curves were obtained using a Time Correlated Single Photon Counting (TCSPC) Spectrophotometer (HORIBA-iHR320) at respective excitation wavelength.

### 2.2.4. General procedure of fluorescence measurement for sensing experiment

To check a typical response for fluorescence intensity towards selective sensing behaviour of FNHNPs for metal ion, we have prepared stock solution of FNHNPs ( $1 \times 10^{-5}$  M) and various metal ions (50  $\mu\text{g}/\text{mL}$ ) in double distilled water. 1 mL stock solution of FNHNPs was added to the 10 mL volumetric flask followed by addition of a known volume of respective metal ion solutions (6 mL). Then the solutions were diluted up to the mark using distilled water (10 mL) so that effective concentration of the metal ion is 30  $\mu\text{g}/\text{mL}$ . These solutions were thoroughly mixed and allowed to maintain room temperature for 5 min. The fluorescence emission spectra of all these solutions were recorded and compared with the spectra of FNHNPs. Surprisingly, selective and sensitive fluorescence intensity change was seen for FNHNPs with addition of  $\text{Cu}^{2+}$  only.

### 2.2.5. Cell culture and fluorescence imaging

The cells MDA-MB-231 and A375 were grown using 10% FBS, penicillin (50 units/mL) and streptomycin (50  $\mu\text{g}/\text{mL}$ ) in DMEM medium at the density  $1 \times 10^5$  cells in 35 mm culture plate. The growth of cells was monitored by feeding a fresh medium each day until it reaches to 60 percentage. Later, the samples viz. FNH in acetone, FNHNPs and FNHNPs +  $\text{Cu}^{2+}$  was treated to the respective cell lines for 24 h with final concentration of 5  $\mu\text{M}$ . During this procedure, cold PBS buffer



**Scheme 2.** Pictorial representation of bathochromic shift in absorbance and fluorescence wavelength of J-aggregated FNHNPs as compared to FNH in acetone.

used two times for the washing. In order to examine the fluorescence images, the cells were systematically observed using the inverted fluorescence microscope (BX51, Olympus, Tokyo, Japan) under blue light (488 nm). The experiment was executed in triplicate at constant exposure time, contrast and brightness settings in humidified atmosphere (95% air and 5% CO<sub>2</sub>) at 37 °C in CO<sub>2</sub> incubator.

#### 2.2.6. Viability assay (MTT)

The MDA-MB-231 and A375 cells were plated and incubated for overnight to the density of  $2.5 \times 10^4$  cells/well in 96-well plates until the growth of cells reaches 60%. The fresh medium was given on each next day to the cells for regular growth. The samples under studies such as FNH in acetone, FNHNPs and FNHNPs + Cu<sup>2+</sup> of 5 μM was

treated with cells separately and allowed to remain undisturbed for 24 h. The PBS buffer used for washing the cells and then further treated with 90 μL of fresh medium and 10 μL of MTT reagent 1 (MTT, 10 mg/mL) to each well of cell line. The addition of 100 μL of MTT reagent 2 (Solubilisation buffer, 10% SDS with 0.01 N HCl and DMSO) to cells further incubate for 4 h at 37 °C in 5% CO<sub>2</sub> incubator. Finally, the absorbance of the samples was recorded using an enzyme-linked immunosorbent assay (ELISA) plate reader at 595 nm.

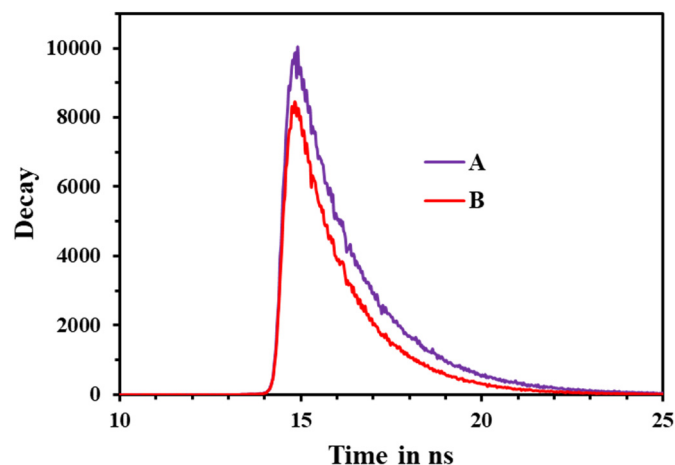


**Fig. 5.** Fluorescence lifetime decay profile of dilute solution of FNH in acetone (A) and aqueous suspension of FNHNPs (B).

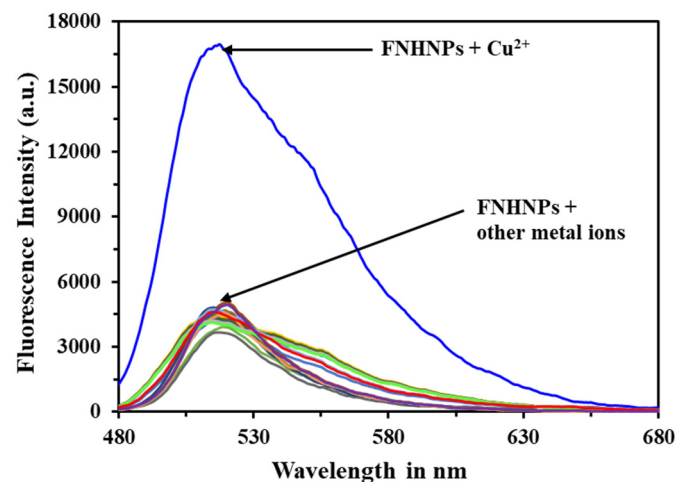


**Fig. 6.** Fluorescence intensity response of FNHNPs in presence of different metal ions (30 μg/mL).

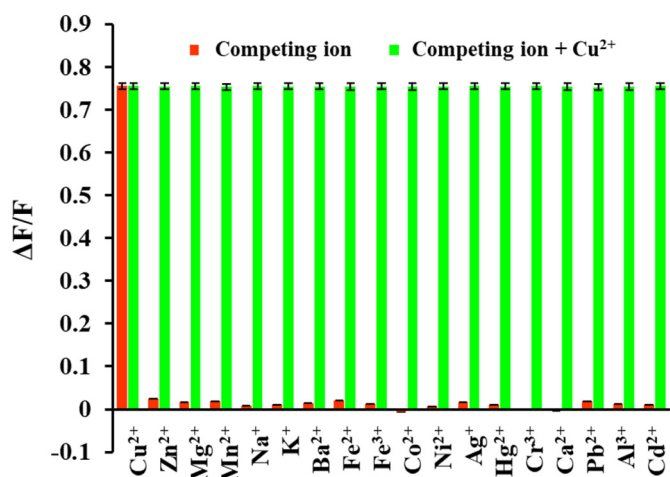


Fig. 7. Relative fluorescence intensity change for respective competing ion in absence and in presence of Cu<sup>2+</sup>.

### 3. Result and discussion

#### 3.1. Particle size, zeta potential and SEM analysis

The various analytical techniques such as particle size analysis, field emission scanning electron microscopy (FE-SEM) and zeta potential measurement were procured for the confirmation of formation and stability of prepared FNHNPs. Fig. 1 shows particle size distribution curve, which clearly indicates uniform and narrow distribution of FNHNPs with average particle size of 58 nm. Fig. 2 indicates the microphotograph of prepared nanoparticles examined on FE-SEM instrument. It seems that the morphology of nanoparticles is distinct spherical shape with slightly different particle size distribution. The size of nanoparticles obtained through FE-SEM analysis is about 60–80 nm which is a close proximity with the size obtained in particle size analysis. The larger particle size observed in FE-SEM analysis is because of possibility of agglomeration of the FNHNPs while preparing air dried film using aqueous suspension of FNHNPs on glass plate for FE-SEM analysis. It is well known that value of zeta potential plays crucial role in a stability factor of aqueous suspension of nanoparticles [40,42,44]. To recognize the surface charge and stability of prepared nanoparticles, zeta potential

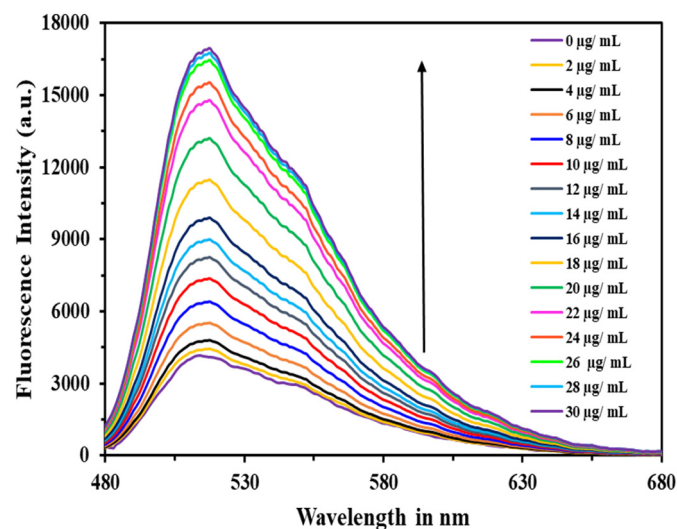


Fig. 8. Fluorescence enhancement of FNHNPs in presence of different concentration of Cu<sup>2+</sup> (0–30 μg/mL).

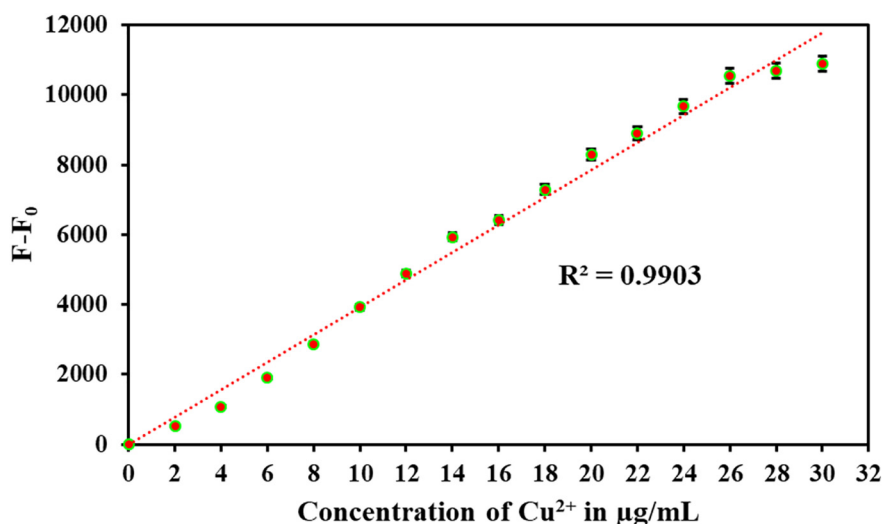


Fig. 9. Digital images under UV lamp and visible light; a-FNH in acetone, b-FNHNPs, c-FNHNPs + 2 μg/mL Cu<sup>2+</sup>, d-FNHNPs + 4 μg/mL Cu<sup>2+</sup>, e-FNHNPs + 8 μg/mL Cu<sup>2+</sup>, f-FNHNPs + 12 μg/mL Cu<sup>2+</sup>, g-FNHNPs + 16 μg/mL Cu<sup>2+</sup>, h-FNHNPs + 20 μg/mL Cu<sup>2+</sup>, i-FNHNPs + 24 μg/mL Cu<sup>2+</sup>, j-FNHNPs + 28 μg/mL Cu<sup>2+</sup>.

analysis was carried out. The zeta potential value found to be  $-31.1$  mV supports the excellent stability and negative charge over the FNHNPs, which is given as Fig. S5. The negative zeta potential directed us the efficacy of FNHNPs as nano probe for the detection of oppositely charged metal ion in an aqueous solution.

#### 3.2. Photophysical properties

The photophysical properties of monomer (FNH in acetone) and nanoparticles (FNHNPs) were examined using UV-Vis. absorption, fluorescence emission and lifetime decay analysis. Fig. 3 shows UV-Vis. absorption spectrum of FNH in acetone (A) and FNHNPs (B). The less pronounced band at 432 nm in absorption spectrum of FNH in acetone (A) and 442 nm in FNHNPs (B) was assigned to the  $\pi \rightarrow \pi^*$  transition. While, broad absorption bands at 452 and 485 nm in FNH in acetone (A) and 477 nm in FNHNPs are due to  $n \rightarrow \pi^*$  transition. The absorption spectrum of prepared nanoparticles peaking at 477 nm is bathochromically shifted as compare to the significant absorption band of parent molecule *i.e.* FNH in acetone at 452 nm. The bathochromic shift in absorption wavelength maxima of FNHNPs is due to the head to tail intermolecular arrangement of monomer units and  $\pi$  stacking effect. The observed red shift in absorption wavelength of nanoparticles supports the formation of J-aggregation of nanoparticles. The fluorescence emission spectra of FNH in acetone (A) and aqueous suspension of FNHNPs (B) shown in Fig. 4. The excitation wavelength of 455 nm was used to scan the fluorescence emission spectra of FNH in acetone (A) and aqueous suspension of FNHNPs (B). The fluorescence emission spectrum of FNH in acetone shows a broad and less intense band peaking at 498 nm is due to  $\pi^* \rightarrow \pi$  transition. However, the red shift in emission wavelength of 20 nm seen for the FNHNPs with increase in the fluorescence intensity, which is assigned to aggregation induced enhanced emission (AIEE). The shifting of zeroth vibrational level of ground electronic state of FNH to a higher vibrational level of excited electronic states arises due to the red shift in emission maxima, formation of J-aggregation pattern in FNHNPs and AIEE phenomenon [45–47]. The remarkable larger Stokes shift of  $\bar{\nu} = 2673.02$  cm<sup>-1</sup> for FNHNPs than FNH in acetone ( $\bar{\nu} = 1897.70$  cm<sup>-1</sup>) also supports the different characteristics of formed material which confirms FNH existence in nano size with significant photophysical properties. The fluorescence emission spectrum of nanoparticles originated from lower excited state display bathochromic shift supports the formation of FNHNPs [45–47]. Scheme 2 shows the pictorial representation of



**Fig. 10.** Calibration curve shows fluorescence enhancement linearity ( $F$  = fluorescence intensity of FNHNPs in presence of  $\text{Cu}^{2+}$  at particular concentration and  $F_0$  = initial fluorescence intensity of FNHNPs in absence of  $\text{Cu}^{2+}$ ).

bathochromic shift in wavelength maxima of absorbance and fluorescence emission of J-aggregated FNHNPs as compared to FNH in acetone. The fluorescence lifetime is one of the vital characteristics property of any fluorescent probe to decide its excited state nature. Fig. 5 indicates lifetime decay curves of FNHNPs (A) and FNH in acetone (B). The longer fluorescence lifetime (4.2 ns) as compared with the FNH in acetone (2.8 ns) is because of restricted molecular rotations and vibrations of molecules in the process of FNHNPs formation which led to decreases the non-radiative pathways.

### 3.3. Effect of pH on fluorescence intensity of FNHNPs

In order to investigate the effect of different pH on the performance of fluorescence intensity of FNHNPs, the fluorescence measurement of FNHNPs in different pH solutions was performed within pH 1 to 12. The results given in Supporting information as Fig. S6. The fluorescence intensity shown by nanoparticles with pH solutions of 6 to 8 is higher than other acidic and basic pH solutions. The disruption of j-aggregated FNH units at extreme acidic or basic conditions results in

**Table 1**

Comparison syntax between reported fluorescent probes and present nano probe with respect to LOD of  $\text{Cu}^{2+}$ .

Sr. no.	Detection method	Molecule based on derivative of	LOD in $\mu\text{M}$	Ref. no.
1.	Fluorescence	Fluorescein	0.296	[1]
2.	Fluorescence	Coumarin	5.80	[15]
3.	Colorimetric/fluorescence	Rhodamine B	3.42	[16]
4.	Fluorescence	Rhodamine	0.0771	[17]
5.	Colorimetric/fluorescence	6G/thiosemicarbazide Bis-(2-pyridylmethyl) amine	0.102	[27]
6.	Fluorescence	Ethylenediamine	0.30	[58]
7.	Fluorescence	Rhodamine B	0.16	[59]
8.	Fluorescence	Rhodamine-diacetic acid conjugate	2.30	[60]
9.	Fluorescence	Rhodamine	0.30	[61]
10.	Fluorescence	Rhodamine	0.039	[62]
11.	Colorimetric/fluorescence	Rhodamine	0.727	[63]
12.	Fluorescence	hydrazone/ferrocene Rhodamine B hydroxylamide	0.033	[64]
13.	Fluorescence	Rhodamine B	0.03	[65]
14.	Fluorescence	Rhodamine	0.28	[66]
15.	Fluorescence	Rhodamine 6G-pyrrole unit	2.94	[67]
16.	Fluorescence	Fluorescein (organic nanoparticles)	0.024	Present work

destabilization of nanoparticles in an aqueous suspension [47]. Therefore, the maximum fluorescence intensity response at neutral *i.e.* pH = 7 led us to choose the ideal pH condition for further sensing experiments.

### 3.4. Selective fluorescence enhancement of FNHNPs by $\text{Cu}^{2+}$

The significant changes observed in fluorescence output of a fluorescent nano probe in presence of analyte molecule become a key factor for design and develop a sensory system. The changes may occur because of interaction of functionalities or surface charge present over the nano probe. In present case, the negative charge over the nanoparticle surface and the functionalities (such as  $-\text{C}=\text{O}$  and  $-\text{NH}$ ) present in basic units of nanoparticles are the fundamental features directs us to examine the utility of FNHNPs as nano probe against 18 metal ion solutions. For this purpose, we tested the fluorescence intensity response of FNHNPs with series of metal ions such as  $\text{Cu}^{2+}$ ,  $\text{Zn}^{2+}$ ,  $\text{Mg}^{2+}$ ,  $\text{Mn}^{2+}$ ,  $\text{Na}^+$ ,  $\text{K}^+$ ,  $\text{Ba}^{2+}$ ,  $\text{Fe}^{2+}$ ,  $\text{Fe}^{3+}$ ,  $\text{Co}^{2+}$ ,  $\text{Ni}^{2+}$ ,  $\text{Ag}^+$ ,  $\text{Hg}^{2+}$ ,  $\text{Cr}^{3+}$ ,  $\text{Ca}^{2+}$ ,  $\text{Pb}^{2+}$ ,  $\text{Al}^{3+}$  and  $\text{Cd}^{2+}$  of 30  $\mu\text{g}/\text{mL}$  concentration each. Fig. 6 shows fluorescence intensity response of FNHNPs in presence of different metal ions. It was found that only  $\text{Cu}^{2+}$  selectively enhances the fluorescence intensity of FNHNPs. While, other metal ions show negligible or very small fluorescence change in case of FNHNPs. The selective fluorescence enhancement is induced by only addition of  $\text{Cu}^{2+}$  solution to FNHNPs is because of strong interaction with the negative charge over the nanoparticle surface having functional groups such as  $-\text{C}=\text{O}$  and  $-\text{NH}$ .

### 3.5. Effect of competing metal ions

The practical applicability of nano probe in establishing the sensor for the detection of metal ion in aqueous solution can be improved through eliminating the effect of other analyte molecules on performance of nanoparticles. To examine the effect of competing metal ions on the fluorescence enhancement of FNHNPs induced by  $\text{Cu}^{2+}$ , each metal ion solution of 30  $\mu\text{g}/\text{mL}$  was added to the solution holding a composite of FNHNPs and  $\text{Cu}^{2+}$  (30  $\mu\text{g}/\text{mL}$ ). All solutions were scanned for fluorescence measurements and results interpreted as relative fluorescence intensity change as  $\Delta F/F_0$ ; where,  $\Delta F$  is difference in fluorescence intensity change after ( $F$ ) and before ( $F_0$ ) addition of competing ion. Fig. 7 indicates the relative fluorescence intensity change for respective competing ion in absence and in presence of  $\text{Cu}^{2+}$ . From the figure, it seems that  $\text{Cu}^{2+}$  induces selective and sensitive fluorescent enhancement for FNHNPs (red color bar, Fig. 7). Whereas other metal ion shows negligible response in fluorescence enhancement of FNHNPs.

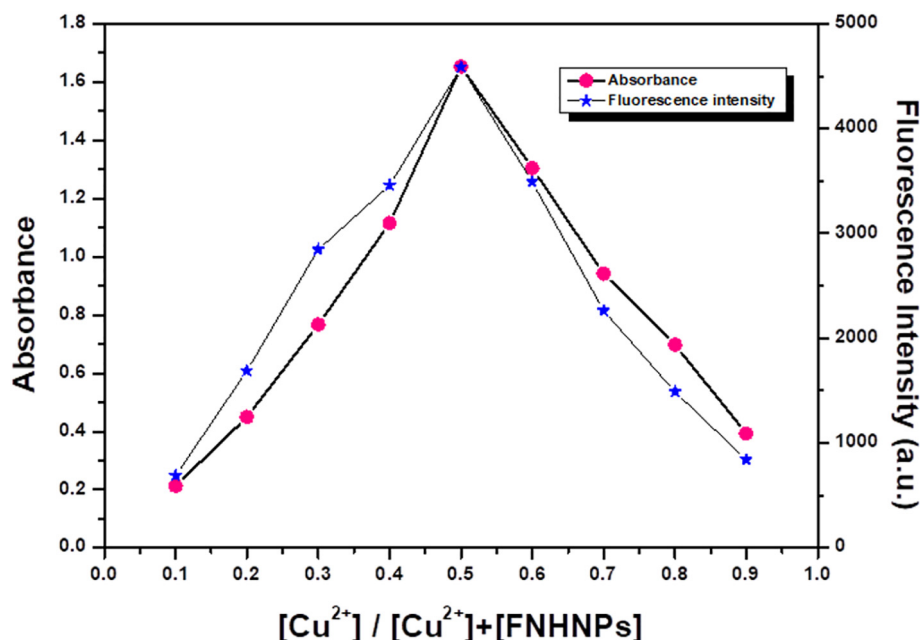


Fig. 11. Job's plot illustrates binding stoichiometry between FNHNPs and Cu<sup>2+</sup>.

The addition of each metal ion to the FNHNPs + Cu<sup>2+</sup> solution does not alter the fluorescence enhancement effect brought by addition of Cu<sup>2+</sup>. The relative fluorescence intensity remains almost same in case of FNHNPs with Cu<sup>2+</sup> and FNHNPs with Cu<sup>2+</sup> in solution of respective metal ion (green color bar, Fig. 7). Thus, repeated experiments indicate that there is no effect of other competing metal ions on fluorescence enhancement of FNHNPs induced by Cu<sup>2+</sup>.

### 3.6. Fluorescence titration of FNHNPs with Cu<sup>2+</sup>

Fig. 8 shows change in fluorescence intensity with increasing concentration of Cu<sup>2+</sup> ion solution from 2 to 30 µg/mL. It was observed that with increasing concentration of Cu<sup>2+</sup> in a solution of FNHNPs, gradually increases the fluorescence intensity. Fig. 8 indicates linear fluorescence intensity response of FNHNPs with increasing amount of Cu<sup>2+</sup> ion. Fig. 9 illustrates the digital photographs of a selected solutions examined under visible and UV lamp (365 nm). From the figure, it is clear that fluorescence intensity of FNHNPs increases with increasing concentration of Cu<sup>2+</sup> to the solution of FNHNPs.

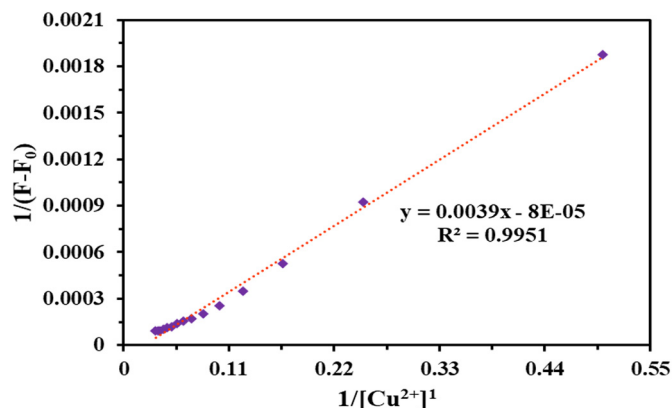


Fig. 12. Modified Benesi-Hildebrand (B-H) plot.

### 3.7. Estimation of statistical parameters

#### 3.7.1. Calibration curve and limit of detection

Fig. 10 shows linearity of fluorescence intensity change with addition of Cu<sup>2+</sup> to FNHNPs. The calibration curve plotted as fluorescence intensity change versus concentration of Cu<sup>2+</sup> ion added. The results were well fitted in straight-line equation and plotted as Fig. 10. The fluorescence enhancement results show linearity in the concentration range of 0–30 µg/mL Cu<sup>2+</sup>. Fig. 10 was used as calibration curve to estimate the lower detection limit (LOD) for Cu<sup>2+</sup> with the help of Eq. (1). LOD was found to be 1.62 ng/mL (0.024 µM).

$$LOD = \frac{3.3\sigma}{K} \tag{1}$$

where, standard deviation and slope of the calibration curve denoted by  $\sigma$  and  $K$ , respectively. The limit of detection estimated by present method is exceptionally lower than the reported fluorescent probes. Table 1 shows comparison statistics of LOD for Cu<sup>2+</sup> using present and some of already reported investigations.

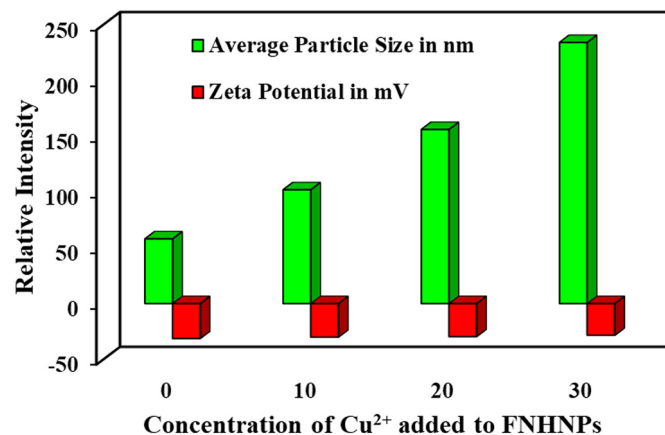


Fig. 13. Variation of zeta potential and particle size distribution of FNHNPs in presence of Cu<sup>2+</sup>.

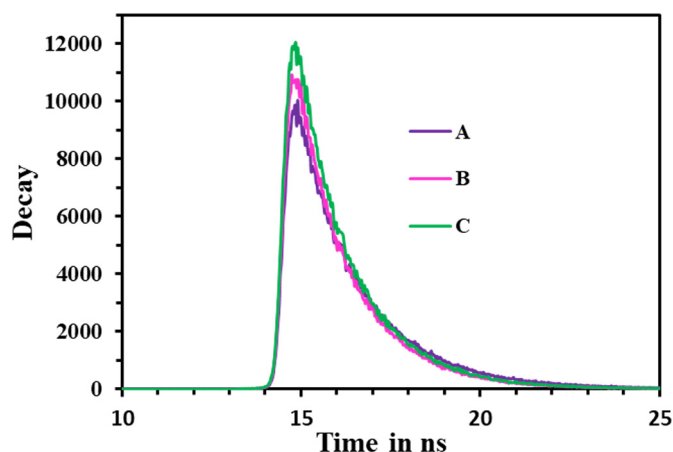


Fig. 14. Lifetime decay curves of FNHNPs in presence of  $\text{Cu}^{2+}$ ; A - FNHNPs, B - FNHNPs + 15  $\mu\text{g}/\text{mL}$  and C - FNHNPs + 30  $\mu\text{g}/\text{mL}$ .

### 3.7.2. Evaluation of stoichiometry and binding constant of complex

The Job's method was used for the investigation of binding parameters between the ligand (FNHNPs) and metal ion ( $\text{Cu}^{2+}$ ) [48,49]. Fig. 11 indicates the absorbance and fluorescence intensity at particular mole fraction (0.1 to 0.9) of  $\text{Cu}^{2+}$  present in respective solution. Fig. 11 is nothing but Job's plot and it shows maximum absorbance and fluorescence intensity in solution of nanoparticle containing 0.5 mole fraction of  $\text{Cu}^{2+}$  that proved 1:1 complexation of FNHNPs and  $\text{Cu}^{2+}$ . The modified Benesi-Hildebrand (B-H) equation [39,42,50,51] used to estimate the binding constant of complex FNHNPs- $\text{Cu}^{2+}$  and given as below.

$$\frac{1}{F - F_0} = \frac{1}{(F_{\text{MAX}} - F_0)} + \frac{1}{K_B(F_{\text{MAX}} - F_0)} \frac{1}{[\text{Cu}^{2+}]^n} \quad (2)$$

where, maximum fluorescence intensity of FNHNPs with  $\text{Cu}^{2+}$ , fluorescence intensity of FNHNPs without  $\text{Cu}^{2+}$  and fluorescence intensity of FNHNPs with  $\text{Cu}^{2+}$  at respective concentration is denoted by  $F_{\text{max}}$ ,  $F_0$  and  $F$ , respectively. The modified Benesi-Hildebrand (B-H) plot given as Fig. 12 is a straight line. The estimated value of binding constant  $K_B = 2.564 \times 10^4$  was calculated using slope of the plot. The higher value of binding constant suggests the strong and efficient binding between FNHNPs and  $\text{Cu}^{2+}$  in aqueous solution.

### 3.8. Mechanism of fluorescence enhancement of FNHNPs by $\text{Cu}^{2+}$

The mechanism behind the fluorescence enhancement of FNHNPs by the addition of  $\text{Cu}^{2+}$  is discussed on strong chelation enhanced

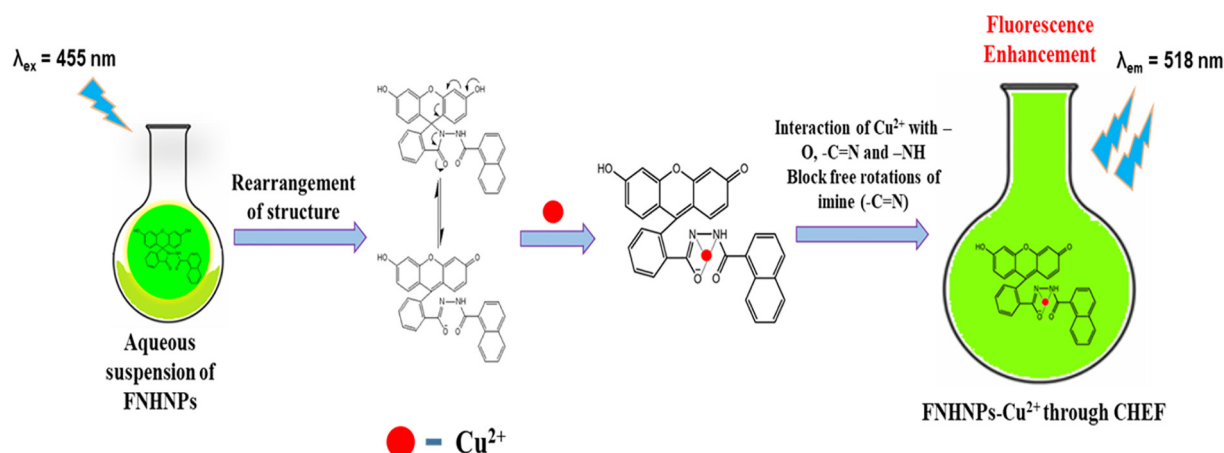
Table 2  
Determination of  $\text{Cu}^{2+}$  in drinking water.

Water samples studied	Amount of standard $\text{Cu}^{2+}$ ion added ( $\mu\text{g}/\text{mL}$ )	Total $\text{Cu}^{2+}$ ion found ( $\mu\text{g}/\text{mL}$ ) (n = 3) <sup>a</sup>	Recovery of $\text{Cu}^{2+}$ ions added (%)	RSD (%)	Relative error (%)
Drinking water <sup>b</sup>	10	9.97	99.70	0.003	-0.3
	20	19.98	99.90	0.004	-0.1
	30	29.97	99.90	0.004	-0.1

<sup>a</sup> n = average of three determinations.

<sup>b</sup> Water sample collected from university campus.

fluorescence phenomenon [39,42,52,53]. To investigate the nature of mechanism involves, a number of experiments were carried out such as UV-Vis. absorption titration, measurement of zeta potential and lifetime decay curves in absence and presence of different concentration of  $\text{Cu}^{2+}$  to FNHNPs. The lone pair of electrons present on oxygen atom of -OH group in xanthene moiety of FNH responsible to open a spiroactam ring and simultaneously rearrange the structure of molecule to form imine bond while addition of  $\text{Cu}^{2+}$  ion to the FNHNPs solution. The interaction of -C=N, -NH and -C=O bonds with  $\text{Cu}^{2+}$  ion restricts the free rotations of imine (-C=N) bond in J-aggregated nanoparticles which simultaneously enhances the fluorescence intensity by means of increase in the radiative pathways [42,54,55]. The complexation between FNHNPs and  $\text{Cu}^{2+}$  ion was confirmed by zeta sizer analysis. Fig. 13 shows variation of particle size and zeta potential of FNHNPs with addition of different concentration of  $\text{Cu}^{2+}$  ion (10, 20 and 30  $\mu\text{g}/\text{mL}$ ). From the results, it is clear that there is only increase in the particle size from 58 nm to 102, 156 and 234 nm with slight change in zeta potential value from -31.3 mV to -30.1, -29.6 and -28.4 mV after the addition of 10, 20 and 30  $\mu\text{g}/\text{mL}$  concentration of  $\text{Cu}^{2+}$ , respectively. The nature of complexation between FNHNPs and  $\text{Cu}^{2+}$  was investigated by using UV-Vis. absorption and fluorescence lifetime decay titration with and without addition of  $\text{Cu}^{2+}$  to FNHNPs. Fig. S7 indicates UV-Vis. absorption spectra of FNHNPs in presence of different concentration of  $\text{Cu}^{2+}$ . Initially, the hypsochromic spectral shift of 12 nm was seen for addition of 2  $\mu\text{g}/\text{mL}$   $\text{Cu}^{2+}$  and then continuous increase in only absorbance value with increasing concentration of  $\text{Cu}^{2+}$  confirms the possibility of excited state interaction between FNHNPs and  $\text{Cu}^{2+}$  ion. The excited state complexation also supported by the evaluation of lifetime decay values. Fig. 14 indicates lifetime decay curves of FNHNPs in absence and presence of different concentration of  $\text{Cu}^{2+}$ . The increase in the lifetime values from 4.2 ns to 4.8 and 5.2 ns with addition of 15  $\mu\text{g}/\text{mL}$  and 30  $\mu\text{g}/\text{mL}$  of  $\text{Cu}^{2+}$  indicates stability and strong complexation ability between FNHNPs and  $\text{Cu}^{2+}$  at excited state. The schematic representation of plausible interaction mode of nanoparticles with  $\text{Cu}^{2+}$  ion illustrated in Scheme 3.



Scheme 3. Plausible interaction mode between FNHNPs with  $\text{Cu}^{2+}$ .

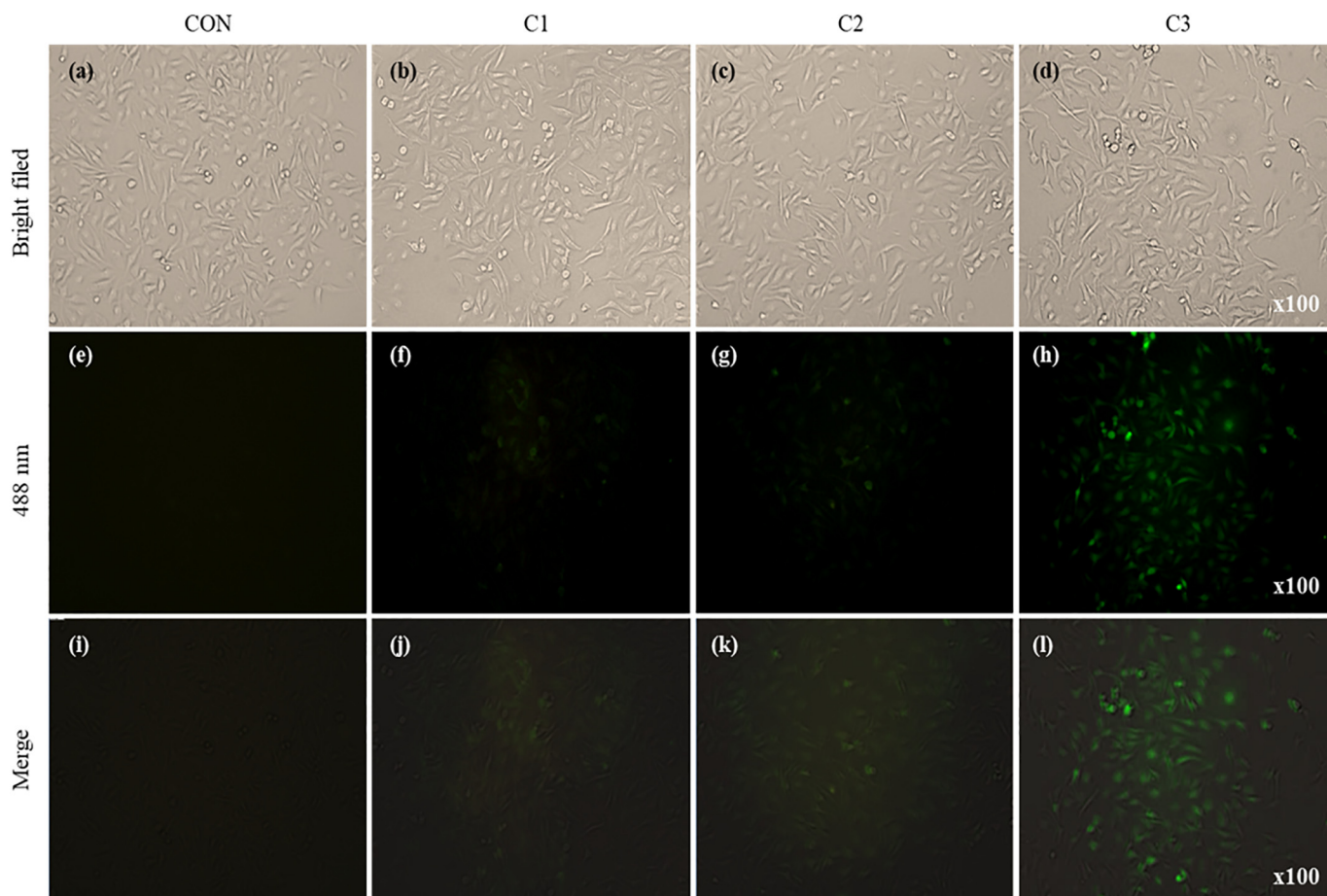


**Fig. 15.** Bright filed transmission images of living MDA-MB-231 cells with control (a), FNH in acetone (b), FNHNPs (c), and FNHNPs + 30  $\mu\text{g/mL}$   $\text{Cu}^{2+}$  (d) and fluorescence images of living MDA-MB-231 cells with control (e), FNH in acetone (f), FNHNPs (g), and FNHNPs + 30  $\mu\text{g/mL}$   $\text{Cu}^{2+}$  (h) by exposing in blue light 488 nm.

### 3.9. Application of proposed sensory method

#### 3.9.1. Quantitative determination of $\text{Cu}^{2+}$ in drinking water analysis

To authenticate the on-site application of proposed sensory method, the prepared FNHNPs were further used for the quantitative analysis of  $\text{Cu}^{2+}$  from drinking water sample. These samples were collected from local campus near the university. First of all, samples were filtered through Whatman filter paper to eliminate the solid impurities. The standard addition method was opted for the preparation of samples in present analysis. For this purpose, three solutions of  $\text{Cu}^{2+}$  ion with different concentration were prepared by spiking standard solution of  $\text{Cu}^{2+}$  (100  $\mu\text{g/mL}$ ). To the 10 mL volumetric flask, 1 mL FNHNPs ( $1 \times 10^{-5}$  M) spiked with required quantity (1, 2 and 3 mL) of standard solution of  $\text{Cu}^{2+}$  and then diluted up to the mark using drinking water so as to final concentration of  $\text{Cu}^{2+}$  in prepared samples were 10, 20 and 30  $\mu\text{g/mL}$ . The samples were measured for fluorescence intensity response and correlated with Fig. 10 as calibration curve to estimate the quantity of  $\text{Cu}^{2+}$  in samples. The results summarized in Table 2 indicates that estimated quantity of  $\text{Cu}^{2+}$  ion in drinking water samples is in close agreement with the spiked quantity of  $\text{Cu}^{2+}$ .

#### 3.9.2. Bioimaging application of FNHNPs for living cells

**3.9.2.1. Cell imaging.** The present FNHNPs probe is highly selective towards the  $\text{Cu}^{2+}$  ion in an aqueous medium through fluorescence enhancement effect. In order to prove the compatibility and practical applicability of present sensory system in bioimaging studies, we have demonstrated the cell imaging study of prepared nanoparticles with

and without addition of  $\text{Cu}^{2+}$  to the cell lines namely MDA-MB-231 and A375. For this purpose, the already cultured cells were treated with the respective samples such as FNH in acetone (C1), FNHNPs (C2) and FNHNPs +  $\text{Cu}^{2+}$  (C3). The reference control (CON) was used to correlate the performance of each sample under studies. The excitation wavelength of blue light i.e. 488 nm was used to produce the fluorescence images. Figs. 15 and 16 show bright filed transmission and fluorescence images (488 nm) of living MDA-MB-231 and A375 cells with the control and respective samples. It is found that fluorescence images presented in both the figures shows higher fluorescence for FNHNPs +  $\text{Cu}^{2+}$  (C3) with respect to the FNH in acetone (C1) and FNHNPs (C2). The parent molecule FNH is hydrophobic in nature that was used to prepare FNHNPs. However, solubility of FNH in acetone implies use of acetone for fluorescence imaging experiment. The interface between domestic existence of  $\text{Cu}^{2+}$  in cell lines and samples such as FNH in acetone or aqueous suspension of FNHNPs shows adequate fluorescence. The addition of external  $\text{Cu}^{2+}$  solution to the FNHNPs significantly variate the fluorescence response and shows noteworthy imaging results. Therefore, based on the present research observations and findings, we conclude that FNHNPs could be the best choice to explore as nano sensor for intracellular copper ion detection.

**3.9.2.2. Cytotoxicity.** The toxic nature of FNH in acetone, FNHNPs and FNHNPs +  $\text{Cu}^{2+}$  towards MDA-MB-231 and A375 cells was examined by cytotoxicity assay. For this study, the cells were treated with the particular concentration of samples i.e. FNH in acetone (C1), aqueous suspension of FNHNPs without (C2) and with presence of  $\text{Cu}^{2+}$  (C3) for 24 h. The MTT assay was used to examine the cell viability [56,57].

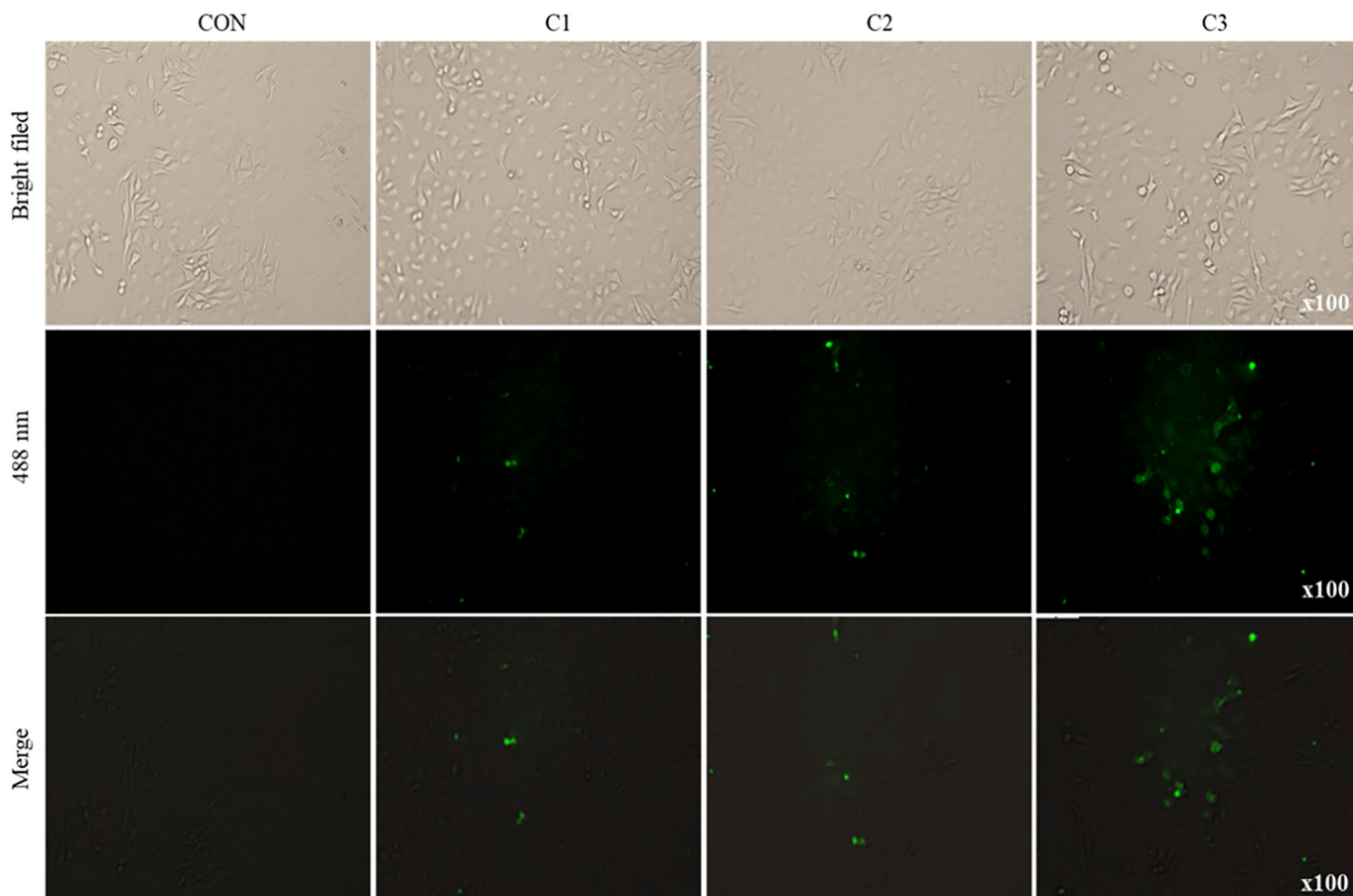


**Fig. 16.** Bright filed transmission images of living A375 cells with control (a), FNH in acetone (b), FNHNPs (c), and FNHNPs + 30 µg/mL Cu<sup>2+</sup> (d) and fluorescence images of living A375 cells with control (e), FNH in acetone (f), FNHNPs (g), and FNHNPs + 30 µg/mL Cu<sup>2+</sup> (h) by exposing in blue light 488 nm.

Figs. 17 and 18 indicate cell viability measurements for MDA-MB-231 and A375 using MTT assay, respectively. The non-toxic behaviour of studied samples was predicted as close count of percentage with the

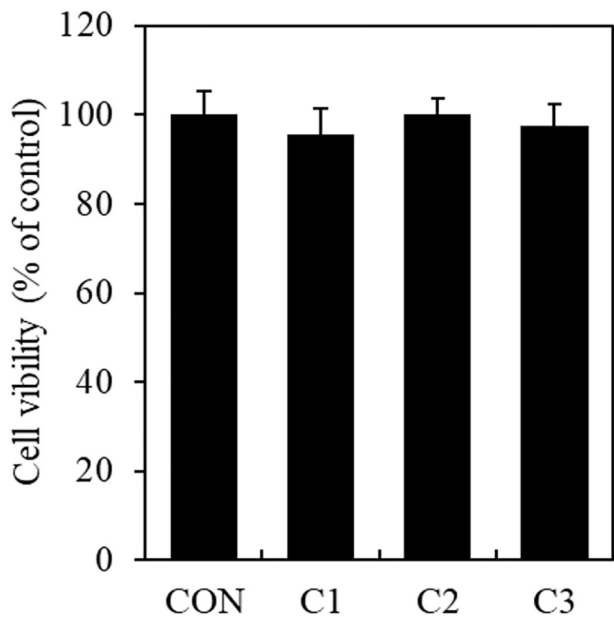


**Fig. 17.** Cell viability measurement using the MTT assay. MDA-MB-231 cells were untreated (Control-CON) or treated with FNH in acetone (C1), FNHNPs (C2), and FNHNPs + 30 µg/mL Cu<sup>2+</sup> (C3) for 24 h.

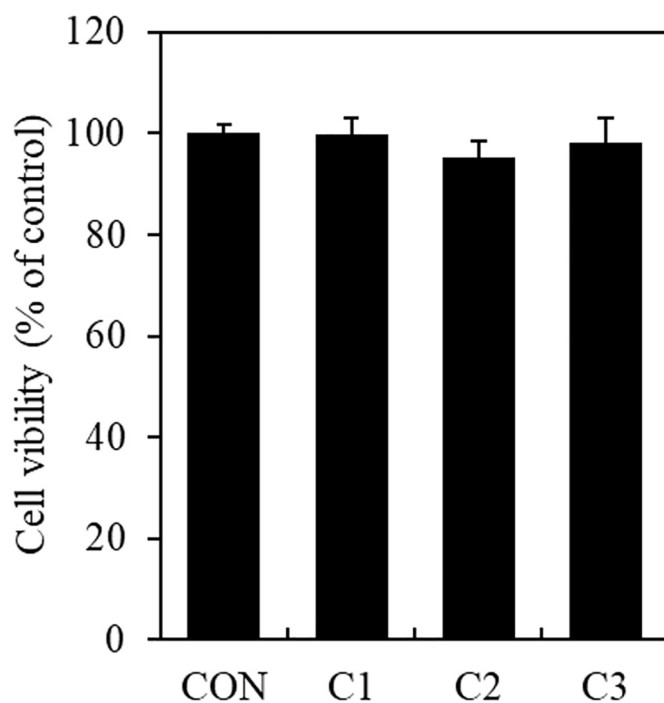


**Fig. 18.** Cell viability measurement using the MTT assay. A375 cells were untreated (Control-CON) or treated with FNH in acetone (C1), FNHNPs (C2), and FNHNPs + 30 µg/mL Cu<sup>2+</sup> (C3) for 24 h.

control. Pleasingly, it found that FNHNPs in absence and presence of  $\text{Cu}^{2+}$  did not shows toxic nature for the MDA-MB-231 and A375 cells. The results observed during cell imaging and cytotoxicity studies summarized that FNHNPs with and without addition with  $\text{Cu}^{2+}$  (C3, h) are more fluorescent, bioactive and useful in comparison with the FNH in acetone (C1, f).

#### 4. Conclusion

A selective and sensitive nano sensor has been developed for the ultra-trace detection of  $\text{Cu}^{2+}$  ion in aqueous solution using fluorescein based organic nanoparticles (FNHNPs). The selective fluorescence enhancement of FNHNPs was observed by the addition of only  $\text{Cu}^{2+}$ . However, other metal ion does not affect the fluorescence outcome induced by  $\text{Cu}^{2+}$ . The fluorescence enhancement found to be linear in concentration range of 2 to 30  $\mu\text{g/mL}$ . The mechanism and the reason for fluorescence enhancement were discussed on excited state complexation between FNHNPs with  $\text{Cu}^{2+}$  ion and chelation enhanced fluorescence (CHEF) phenomenon. The exceptionally lower detection limit for  $\text{Cu}^{2+}$  found to be 1.62  $\text{ng/mL}$  (0.024  $\mu\text{M}$ ) in aqueous solution is an advantage over the traditional fluorescent probes. The present study successfully applied for the quantitative determination of  $\text{Cu}^{2+}$  in drinking water sample. In addition, the excellent intracellular cell imaging capacity of FNHNPs for  $\text{Cu}^{2+}$  and non-toxic performance towards MDA-MB-231 and A375 cells specifies their diverse applicability. Thus, the excellent hydrophilic nature, selective binding ability towards  $\text{Cu}^{2+}$ , photophysical properties and practical applicability of FNHNPs suggests exploration of FNHNPs can be possible as biological marker in environmental as well as cell imaging samplings.

#### Acknowledgement

This research has been performed as a cooperation project of “Enhancement of Korea Chemical Bank” and supported by the Korea Research Institute of Chemical Technology (KRICT).

#### Appendix A. Supplementary data

Supplementary data to this article can be found online at <https://doi.org/10.1016/j.saa.2019.03.021>.

#### References

- [1] X. Bao, Q. Cao, X. Wu, H. Shu, B. Zhou, Y. Geng, J. Zhu, Design and synthesis of a new selective fluorescent chemical sensor for  $\text{Cu}^{2+}$  based on a Pyrrole moiety and a Fluorescein conjugate, *Tetrahedron Lett.* 57 (2016) 942–948, <https://doi.org/10.1016/j.tetlet.2016.01.056>.
- [2] X. Jin, L. Hao, Y. Hu, M. She, Y. Shi, M. Obst, J. Li, Z. Shi, Two novel fluorescein-based fluorescent probes for hypochlorite and its real applications in tap water and biological imaging, *Sens. Actuat. B* 186 (2013) 56–60, <https://doi.org/10.1016/j.snb.2013.05.079>.
- [3] C. Queirós, A.M.G. Silva, S.C. Lopes, G. Ivanova, P. Gameiro, M. Rangel, A novel fluorescein-based dye containing a catechol chelating unit to sense iron(III), *Dyes Pigments* 93 (2012) 1447–1455, <https://doi.org/10.1016/j.dyepig.2011.10.010>.
- [4] B.D. Vanjare, P.G. Mahajan, S.K. Hong, K.H. Lee, Discriminating chemo-sensor for detection of  $\text{Fe}^{3+}$  in aqueous media by fluorescence quenching methodology, *Bull. Kor. Chem. Soc.* 39 (2018) 631–637, <https://doi.org/10.1002/bkcs.11442>.
- [5] D. Shi, F. Yan, M. Wang, Y. Zou, T. Zheng, X. Zhou, L. Chen, Rhodamine derivative functionalized chitosan as efficient sensor and adsorbent for mercury (II) detection and removal, *Mater. Res. Bull.* 70 (2015) 958–964, <https://doi.org/10.1016/j.materresbull.2015.06.046>.
- [6] Z. Wu, Q. Chen, G. Yang, C. Xiao, J. Liu, S. Yang, J.S. Ma, Novel fluorescent sensor for Zn(II) based on bis(pyrrol-2-yl-methyleneamine) ligands, *Sensors Actuators B Chem.* 99 (2004) 511–515, <https://doi.org/10.1016/j.snb.2003.12.070>.
- [7] X. Bao, Q. Cao, X. Nie, Y. Zhou, R. Ye, B. Zhou, J. Zhu, Design and synthesis of a novel chromium(III) selective fluorescent chemosensor bearing a thioacetamide moiety and two rhodamine B fluorophores, *Sensors Actuators B Chem.* 221 (2015) 930–939, <https://doi.org/10.1016/j.snb.2015.07.060>.
- [8] X.-J. Liu, M. Zhang, M.-P. Yang, B. Li, Z. Cheng, B.-Q. Yang, Low cytotoxicity rhodamine-based fluorescent probes for Fe (III) and their application in living cells, *Tetrahedron* 71 (2015) 8194–8199, <https://doi.org/10.1016/j.tet.2015.08.031>.
- [9] Y. Wang, H.Q. Chang, W.N. Wu, W.B. Peng, Y.F. Yan, C.M. He, T.T. Chen, X.L. Zhao, Z.Q. Xu, Rhodamine 6G hydrazone bearing pyrrole unit: ratiometric and selective fluorescent sensor for  $\text{Cu}^{2+}$  based on two different approaches, *Sens. Actuat. B* 228 (2016) 395–400, <https://doi.org/10.1016/j.snb.2016.01.052>.
- [10] L. Zhang, X. Zhang, A selectively fluorescein-based colorimetric probe for detecting copper(II) ion, *Spectrochim. Acta A: Mol. Biomol. Spectroscopy* 133 (2014) 54–59, <https://doi.org/10.1016/j.saa.2014.04.130>.
- [11] M. Yu, M. Shi, Z. Chen, F. Li, X. Li, Y. Gao, J. Xu, H. Yang, Z. Zhou, T. Yi, C. Huang, Highly sensitive and fast responsive fluorescence turn-on chemodosimeter for  $\text{Cu}^{2+}$  and its application in live cell imaging, *Chem. Eur. J.* 14 (2008) 6892–6900, <https://doi.org/10.1002/chem.200800005>.
- [12] W.J. Xu, D.Q. Qi, J.Z. You, F.F. Hu, J.Y. Bian, C.X. Yang, J. Huang, Coumarin based ‘turn-off’ fluorescent chemosensor with high selectivity for  $\text{Cu}^{2+}$  in aqueous solution, *J. Mol. Struct.* 1091 (2015) 133–137, <https://doi.org/10.1016/j.molstruc.2015.02.083>.
- [13] X. Wang, J. Tao, X. Chen, H. Yang, An ultrasensitive and selective “off-on” rhodamine-based colorimetric and fluorescent chemodosimeter for the detection of  $\text{Cu}^{2+}$ , *Sens. Actuat. B* 244 (2017) 709–716, <https://doi.org/10.1016/j.snb.2017.01.040>.
- [14] F. Ye, Q. Chai, X.M. Liang, M.Q. Li, Z.Q. Wang, Y. Fu, A highly selective and sensitive fluorescent turn-off probe for  $\text{Cu}^{2+}$  based on a guanidine derivative, *Molecules* 22 (2017) 1741, <https://doi.org/10.3390/molecules22101741>.
- [15] H.Q. Chang, X.L. Zhao, W.N. Wu, L. Jia, Y. Wang, A highly sensitive on-off fluorescent chemosensor for  $\text{Cu}^{2+}$  based on coumarin, *J. Luminescence* 182 (2017) 268–273, <https://doi.org/10.1016/j.jlumin.2016.10.041>.
- [16] Z. Xu, L. Zhang, R. Guo, T. Xiang, C. Wu, Z. Zheng, F. Yang, A highly sensitive and selective colorimetric and off-on fluorescent chemosensor for  $\text{Cu}^{2+}$  based on rhodamine B derivative, *Sens. Actuat. B* 156 (2011) 546–552, <https://doi.org/10.1016/j.snb.2011.01.066>.
- [17] Y. Wang, H.Q. Chang, W.N. Wu, X.J. Mao, X.L. Zhao, Y. Yang, Z.Q. Xu, Z.H. Xu, L. Jia, A highly sensitive and selective colorimetric and off-on fluorescent chemosensor for  $\text{Cu}^{2+}$  based on rhodamine 6G hydrazone bearing thiosemi-carbazide moiety, *J. Photochem. Photobiol. A Chem.* 335 (2017) 10–16, <https://doi.org/10.1016/j.jphtchem.2016.11.003>.
- [18] P.C. Crooker, N. Garrido, G.A. Ahearn, Copper transport by lobster hepato-pancreatic epithelial cells separated by centrifugal elutriation: measurements with the fluorescent dye Phen green, *J. Exp. Biol.* 204 (2001) 1433–1444, <http://jeb.biologists.org/content/204/8/1433.long>.
- [19] W. Breuer, S. Epsztejn, P. Millgram, I.Z. Cabantchik, Transport of iron and other transition metals into cells as revealed by a fluorescent probe, *Am. J. Phys.* 268 (1995) C1354–C1361, <https://doi.org/10.1152/ajpcell.1995.268.6.C1354>.
- [20] T. Li, Z. Yang, Y. Li, Z. Liu, G. Qi, B. Wang, A novel fluorescein derivative as a colorimetric chemosensor for detecting copper(II) ion, *Dyes Pigments* 88 (2011) 103–108, <https://doi.org/10.1016/j.dyepig.2010.05.008>.
- [21] R. Corradini, A. Dossena, G. Galaverna, R. Marchelli, A. Panagia, G.J. Sartor, Fluorescent chemosensor for organic guests and copper(II) ion based on dansyl-diethylenetriamine-modified  $\beta$ -cyclodextrin, *J. Org. Chem.* 62 (1997) 6283–6289, <https://doi.org/10.1021/jo970349d>.
- [22] W.Y. Lin, H.E. Van Wart, Effect of metal ions on the fluorescence of leucine aminopeptidase and its dansyl-peptide substrates, *J. Inorg. Biochem.* 32 (1998) 21–38, [https://doi.org/10.1016/0162-0134\(88\)80013-8](https://doi.org/10.1016/0162-0134(88)80013-8).
- [23] L. Fabbri, M. Licchelli, P. Pallavicini, A. Perotti, A. Taglietti, D. Sacchi, Fluorescent sensors for transition metals based on electron transfer and energy transfer mechanisms, *Chem. Eur. J.* 2 (1996) 75–82, <https://doi.org/10.1002/chem.19960020114>.
- [24] L. Fabbri, M. Licchelli, P. Pallavicini, A. Perotti, A. Taglietti, D. Sacchi, Ein Fluoreszenzsensor für Übergangsmetall-Ionen auf Anthracenbasis, *Angew. Chem.* 106 (1994) 2051–2053, <https://doi.org/10.1002/ange.19941061923>.
- [25] Z.Q. Zhu, Y.Y. Su, J. Li, D. Li, J. Zhang, S.P. Song, Y. Zhao, G.X. Li, C.H. Fan, Highly sensitive electrochemical sensor for mercury(II) ions by using a mercury-specific oligonucleotide probe and gold nanoparticle-based amplification, *Anal. Chem.* 81 (2009) 7660–7666, <https://doi.org/10.1021/ac9010809>.
- [26] N. Niammont, A. Khumsri, A. Promchat, G. Tumcharern, M. Sukwattanasinitt, Novel salicylaldehyde derivatives as fluorescence turn-on sensors for cyanide ion, *J. Hazard. Mater.* 280 (2014) 458–463, <https://doi.org/10.1016/j.jhazmat.2014.08.028>.
- [27] D. Chen, P. Chen, L. Zong, Y. Sun, G. Liu, X. Yu, J. Qin, Colorimetric and fluorescent probes for real-time naked eye sensing of copper ion in solution and on paper substrate, *R. Soc. Open Sci.* 4 (2017) , 171161 <https://doi.org/10.1098/rsos.171161>.
- [28] N. Pourreza, R. Hoveizavi, Simultaneous preconcentration of Cu, Fe and Pb as methylthymol blue complexes on naphthalene adsorption and flame atomic absorption determination, *Anal. Chim. Acta* 549 (2005) 124–128, <https://doi.org/10.1016/j.aca.2005.06.037>.
- [29] T.W. Lin, S.D. Huang, Direct and simultaneous determination of copper, chromium, aluminum, and manganese in urine with a multielement graphite furnace atomic absorption spectrometer, *Anal. Chem.* 73 (2001) 4319–4325, <https://doi.org/10.1021/ac010319h>.
- [30] B. Tang, J.Y. Niu, C.G. Yu, L.H. Zhuo, J.C. Ge, Highly luminescent water-soluble Cd Te nanowires as fluorescent probe to detect copper (II), *Chem. Commun.* (33) (2005) 4184–4186, <https://doi.org/10.1039/B502978C>.
- [31] A. Mokhir, A. Kiel, D.P. Herten, R. Kraemer, Fluorescent sensor for  $\text{Cu}^{2+}$  with a tunable emission wavelength, *Inorg. Chem.* 44 (2005) 5661–5666, <https://doi.org/10.1021/ic050362d>.
- [32] I. Tomalova, P. Foltynova, V. Kanicky, J. Preisler, MALDI MS and ICP MS detection of a single CE separation record: a tool for metalloproteomics, *Anal. Chem.* 86 (2014) 647–654, <https://doi.org/10.1021/ac402941e>.
- [33] Y. Liu, P. Liang, L. Guo, Nanometer titanium dioxide immobilized on silica gel as sorbent for preconcentration of metal ions prior to their determination by inductively

- coupled plasma emission spectrometry, *Talanta* 68 (2005) 25–30, <https://doi.org/10.1016/j.talanta.2005.04.035>.
- [34] J.S. Becker, M.V. Zoriy, C. Pickhardt, G.N. Palomer, K. Zilles, Imaging of copper, zinc, and other elements in thin section of human brain samples (hippocampus) by laser ablation inductively coupled plasma mass spectrometry, *Anal. Chem.* 77 (2005) 3208–3216, <https://doi.org/10.1021/ac040184q>.
- [35] X. Chen, T. Pradhan, F. Wang, J.S. Kim, J. Yoon, Fluorescent chemosensors based on spiroring-opening of xanthenes and related derivatives, *Chem. Rev.* 112 (2012) 1910–1956, <https://doi.org/10.1021/cr200201z>.
- [36] J. Hatai, S. Pal, S. Bandyopadhyay, Fluorescent detection of silver ions in water with organic nano-aggregates, *RSC Adv.* 2 (2012) 10941–10947, <https://doi.org/10.1039/C2RA21717A>.
- [37] J. Wang, X. Xu, L. Shi, L. Li, Fluorescent organic nanoparticles based on branched small molecule: preparation and ion detection in lithium-ion battery, *ACS Appl. Mater. Interfaces* 5 (2013) 3392–3400, <https://doi.org/10.1021/am4004396>.
- [38] B.K. An, S.K. Kwon, S.D. Jung, S.Y. Park, Enhanced emission and its switching in fluorescent organic nanoparticles, *J. Am. Chem. Soc.* 124 (2002) 14410–14415, <https://doi.org/10.1021/ja0269082>.
- [39] P.G. Mahajan, D.P. Bhopate, G.B. Kolekar, S.R. Patil, N-methyl isatin nanoparticles as a novel probe for selective detection of Cd<sup>2+</sup> ion in aqueous medium based on chelation enhanced fluorescence and application to environmental sample, *Sensors Actuators B* 220 (2015) 864–872, <https://doi.org/10.1016/j.snb.2015.05.119>.
- [40] P.G. Mahajan, N.C. Dige, N.K. Desai, S.R. Patil, V.V. Kondalkar, S.K. Hong, K.H. Lee, Selective detection of Co<sup>2+</sup> by fluorescent nano probe: diagnostic approach for analysis of environmental samples and biological activities, *Spectrochim. Acta A: Molecul. Biomol. Spectroscop* 198 (2018) 136–144, <https://doi.org/10.1016/j.saa.2018.03.004>.
- [41] P.G. Mahajan, G.B. Kolekar, S.R. Patil, Recognition of D-penicillamine using Schiff base centered fluorescent organic nanoparticles and application to medicine analysis, *J. Fluoresc.* 27 (2017) 829–839, <https://doi.org/10.1007/s10895-016-2019-5>.
- [42] P.G. Mahajan, N.C. Dige, B.D. Vanjare, Y. Han, S.J. Kim, S.K. Hong, K.H. Lee, Intracellular imaging of zinc ion in living cells by fluorescein based organic nanoparticles, *Sensors Actuators B* 267 (2018) 119–128, <https://doi.org/10.1016/j.snb.2018.03.186>.
- [43] P.G. Mahajan, G.B. Kolekar, S.R. Patil, Recognition of D-Penicillamine Using Schiff Base Centered Fluorescent Organic Nanoparticles and Application to Medicine Analysis, *J. Fluoresc.* 27 (2017) 829–839, <https://doi.org/10.1007/s10895-016-2019-5>.
- [44] J. Lyklema, *Fundamentals of Interface and Colloid Science*, Elsevier, Wageningen, 1995.
- [45] F. Wang, M. Han, M. Yi, Y. Wang, Y. Lai, Aggregation driven growth of size-tunable organic nanoparticles using electronically altered conjugated polymers, *J. Am. Chem. Soc.* 127 (2005) 10350–10355, <https://doi.org/10.1021/ja0521730>.
- [46] X. Zhang, X. Zhang, S. Wang, M. Liu, L. Tao, Y. Wei, Surfactant modification of aggregation-induced emission material as biocompatible nanoparticles: facile preparation and cell imaging, *Nanoscale* 5 (2013) 147–150, <https://doi.org/10.1039/C2NR32698A>.
- [47] P.G. Mahajan, N.K. Desai, D.K. Dalavi, D.P. Bhopate, G.B. Kolekar, S.R. Patil, Cetyltrimethylammonium bromide capped 9-anthraldehyde nanoparticles for selective recognition of phosphate anion in aqueous solution based on fluorescence quenching and application for analysis of chloroquine, *J. Fluoresc.* 25 (2015) 31–38, <https://doi.org/10.1007/s10895-014-1451-7>.
- [48] J.M. Jung, S.Y. Lee, E. Nam, M.H. Lim, C. Kim, A highly selective turn-on chemosensor for Zn<sup>2+</sup> in aqueous media and living cells, *Sensors Actuators B Chem.* 244 (2017) 1045–1053, <https://doi.org/10.1016/j.snb.2017.01.076>.
- [49] P. Job, Formation and stability of inorganic complexes in solution, *Ann. Chim.* 9 (1928) 113–203.
- [50] A. Samanta, N. Guchhait, S.C. Bhattacharya, A simple but highly selective and sensitive fluorescence reporter for toxic Cd (II) ion via excimer formation, *Chem. Phys. Lett.* 612 (2014) 251–255, <https://doi.org/10.1016/j.cplett.2014.08.034>.
- [51] H.A. Benesi, J.H. Hildebrand, A spectrophotometric investigation of the interaction of iodine with aromatic hydrocarbons, *J. Am. Chem. Soc.* 71 (1949) 2703–2707, <https://doi.org/10.1021/ja01176a030>.
- [52] L.N. Wang, W.W. Qin, W.S. Liu, A sensitive Schiff-base fluorescent indicator for the detection of Zn<sup>2+</sup>, *Inorg. Chem. Commun.* 13 (2010) 1122–1125, <https://doi.org/10.1016/j.inoche.2010.06.021>.
- [53] M. Kumar, A. Kumar, M. Kumar Singh, S.K. Sahu, R.P. John, A novel benzidine based Schiff base turn-on fluorescent chemosensor for selective recognition of Zn<sup>2+</sup>, *Sensors Actuators B Chem.* 241 (2017) 1218–1223, <https://doi.org/10.1016/j.snb.2016.10.008>.
- [54] J.S. Wu, W.M. Liu, X.Q. Zhuang, F. Wang, P.F. Wang, S.L. Tao, X.H. Zhang, S.K. Wu, S.T. Lee, Fluorescence turn on of coumarin derivatives by metal cations: a new signalling mechanism based on CN isomerization, *Org. Lett.* 9 (2007) 33–36, <https://doi.org/10.1021/ol062518z>.
- [55] P.S. Hariharan, S.P. Anthony, Substitutional group dependent colorimetric/fluorimetric sensing of Mn<sup>2+</sup>, Fe<sup>3+</sup> and Zn<sup>2+</sup> ions by simple Schiff base chemosensor, *Spectrochim. Acta Part A: Mol. Biomol. Spectrosc.* 136 (2015) 1658–1665, <https://doi.org/10.1016/j.saa.2014.10.061>.
- [56] A.R. Phull, S.H. Eo, S.J. Kim, Oleonic acid (OA) regulates inflammation and cellular dedifferentiation of chondrocytes via MAPK signaling pathways, *Cell. Mol. Biol. (Noisy le Grand)* 63 (2017) 12–17, <https://doi.org/10.14715/cmb/2017.63.3.3>.
- [57] A.R. Phull, M. Majid, I.U. Haq, M.R. Khan, S.J. Kim, In vitro and in vivo evaluation of anti-arthritis, antioxidant efficacy of fucoidan from *Undaria pinnatifida* (Harvey) Suringar, *Int. J. Biol. Macromol.* 97 (2017) 468–480, <https://doi.org/10.1016/j.ijbiomac.2017.01.051>.
- [58] S.H. Yun, L. Xia, T.N. Jebakumar, I. Edison, M. Pandurangan, D.H. Kim, S.H. Kim, Y.R. Lee, Highly selective fluorescence turn-on sensor for Cu<sup>2+</sup> ions and its application in confocal imaging of living cells, *Sens. Actuat. B* 240 (2017) 988–995, <https://doi.org/10.1016/j.snb.2016.09.070>.
- [59] M. Saleem, K.H. Lee, Selective fluorescence detection of Cu<sup>2+</sup> in aqueous solution and living cells, *J. Luminesc.* 145 (2014) 843–848, <https://doi.org/10.1016/j.jlumin.2013.08.044>.
- [60] S. Goswami, D. Sen, A.K. Das, N.K. Das, K. Aich, H.K. Fun, C.K. Quah, A.K. Maity, P. Saha, A new rhodamine-coumarin Cu<sup>2+</sup> selective colorimetric and ‘off-on’ fluorescence probe for effective use in chemistry and bioimaging along with its bound X-ray crystal structure, *Sensors Actuators B Chem.* 183 (2013) 518–525, <https://doi.org/10.1016/j.snb.2013.04.005>.
- [61] X. Zeng, L. Dong, C. Wu, L. Mu, S.F. Xue, Z. Tao, Highly sensitive chemosensor for Cu (II) and Hg (II) based on the tripodalrhodamine receptor, *Sensors Actuators B Chem.* 141 (2009) 506–510, <https://doi.org/10.1016/j.snb.2009.07.013>.
- [62] J. Jeong, B.A. Rao, Y.A. Son, Dual sensing performance of a rhodamine derived scaffold for the determination of Cu<sup>2+</sup> and Ce<sup>4+</sup> in aqueous media, *Sensors Actuators B Chem.* 220 (2015) 1254–1265, <https://doi.org/10.1016/j.snb.2015.07.048>.
- [63] F. Ge, H. Ye, J.Z. Luo, S. Wang, Y.J. Sun, B.X. Zhao, J.Y. Miao, A new fluorescent and colorimetric chemosensor for Cu(II) based on rhodamine hydrazone and ferrocene unit, *Sensors Actuators B Chem.* 181 (2013) 215–220, <https://doi.org/10.1016/j.snb.2013.01.048>.
- [64] X. Chen, J. Jia, H. Ma, S. Wang, X. Wang, Characterization of rhodamine B hydroxylamide as a highly selective and sensitive fluorescence probe for copper (II), *Anal. Chim. Acta* 632 (2009) 9–14, <https://doi.org/10.1016/j.aca.2007.08.025>.
- [65] J. Xu, Y. Hou, Q. Ma, X. Wu, S. Feng, J. Zhang, Y. Shen, A highly selective fluorescent probe for Cu<sup>2+</sup> based on rhodamine B derivative, *Spectrochim. Acta A* 124 (2014) 416–422, <https://doi.org/10.1016/j.saa.2014.01.046>.
- [66] P. Puangpoy, S. Smanmoo, W. Surareungchai, A new rhodamine derivative based chemosensor for highly selective and sensitive determination of Cu<sup>2+</sup>, *Sensors Actuators B Chem.* 193 (2014) 679–686, <https://doi.org/10.1016/j.snb.2013.12.037>.
- [67] Y. Wang, H.Q. Chang, W.N. Wu, W.B. Peng, Y.F. Yan, C.M. He, T.T. Chen, X.L. Zhao, Z.Q. Xu, Rhodamine 6G hydrazone bearing pyrrole unit: ratiometric and selective fluorescent sensor for Cu<sup>2+</sup> based on two different approaches, *Sensors Actuators B Chem.* 228 (2016) 395–400, <https://doi.org/10.1016/j.snb.2016.01.052>.